Mesoscale Convective Systems in relation to African and Tropical Easterly Jets

Lucas Besson, Yvon Lemaître

Mesoscale Convective Systems in Relation to African and Tropical Easterly Jets

L. BESSON AND Y. LEMAÎTRE

Université Versailles St-Quentin, Sorbonne Universités, UPMC Universite Paris 06, CNRS/INSU, LATMOS-IPSL, Guyancourt, France

(Manuscript received 31 July 2013, in final form 22 April 2014)

ABSTRACT

This paper documents the interaction processes between mesoscale convective systems (MCS), the tropical easterly jet (TEJ), and the African easterly jet (AEJ) over West Africa during the monsoon peak of 2006 observed during the African Monsoon Multidisciplinary Analyses (AMMA) project. The results highlight the importance of the cloud system localization relative to the jets in order to explain their duration and life cycle. A systematical study reveals that intense and long-lived MCSs correspond to a particular pattern where clouds associated with deep convection are located in entrance regions of TEJ and in exit regions of AEJ. A case study on a particularly well-documented convective event characterizes this link and infers the importance of jet streaks in promoting areas of divergence, favoring the persistence of MCSs.

1. Introduction

The understanding of the life cycle of African mesoscale convective systems (MCSs) is an important goal of the African Monsoon Multidisciplinary Analyses (AMMA) field campaign, carried out during the West African monsoon (WAM) season in 2006; especially relevant for the forecast of Sahelian precipitation. Indeed, the contribution of MCSs to the annual rainfall amounts ranges from 16% to 32% along the shore of the Gulf of Guinea (Acheampong 1982; Bayo Omotosho 1985), is about 50% in the Sudanian zone (Eldridge 1957; Bayo Omotosho 1985), and is more than 80% in the Sahelian region (Dhonneur 1981; Mohr et al. 1999). This rainfall has been shown to be strongly modulated by the organization and the intensity of deep convection within these MCSs (Fink and Reiner 2003).

In the past, numerous studies have highlighted the crucial role of orography in the initiation of these African MCSs; in particular above the Jos Plateau (Nigeria), the Aïr mountains (Niger), the Darfur mountains (Sudan), and the Ethiopian Highlands (Tetzlaff and Peters 1988; Laing and Fritsch 1993; Redelsperger et al. 2002; Laing et al. 2008; Rickenbach et al. 2009). Other works suggest an important role of dynamical entities such as the African easterly jet (AEJ), the tropical easterly jet (TEJ) (see Fig. 1), African easterly waves (AEWs), and of the convergence term of horizontal moisture flux convergence (Reiter 1969; Payne and McGarry 1977; Bolton 1984; Bayo Omotosho 1984; Machado et al. 1993; Rowell and Milford 1993; Druyan and Hall 1996; Thorncroft and Blackburn 1999; Diongue et al. 2002; Redelsperger et al. 2002; Nicholson and Grist 2003; Mohr and Thorncroft 2006; Laing et al. 2008). However, the physical processes involved are not fully understood.

The midtropospheric AEJ (usually between 700 and 500 hPa) results from the horizontal temperature gradient between the low temperature area over the Gulf of Guinea and the high temperatures over the Sahara (Burpee 1972; Thorncroft and Blackburn 1999; Cook 1999). According to Newell and Kidson (1984) and Grist and Nicholson (2001), the jet intensity is directly related to the moisture content of the monsoon, a slower (faster) speed being related to a wetter (drier) monsoon. The intraseasonal oscillations of the AEJ have an impact on the latitudinal location of the MCSs. A more northern (southern) location of the AEJ leads to a shift of the MCS tracks northward (southward) (Nieto-Ferreira et al. 2009). Nicholls and Mohr (2010) performed a detailed analysis of the local and regional environments of intense convective systems using soundings, operational analysis, and space-based datasets. The speed of the AEJ, the magnitude of the low-level shear, and the surface equivalent potential temperature tend to exhibit larger values

Corresponding author address: Lucas Besson, LATMOS-IPSL, 4 place Jussieu, 75005 Paris, France.
E-mail: lucas.besson@latmos.ipsl.fr

DOI: 10.1175/MWR-D-13-00247.1

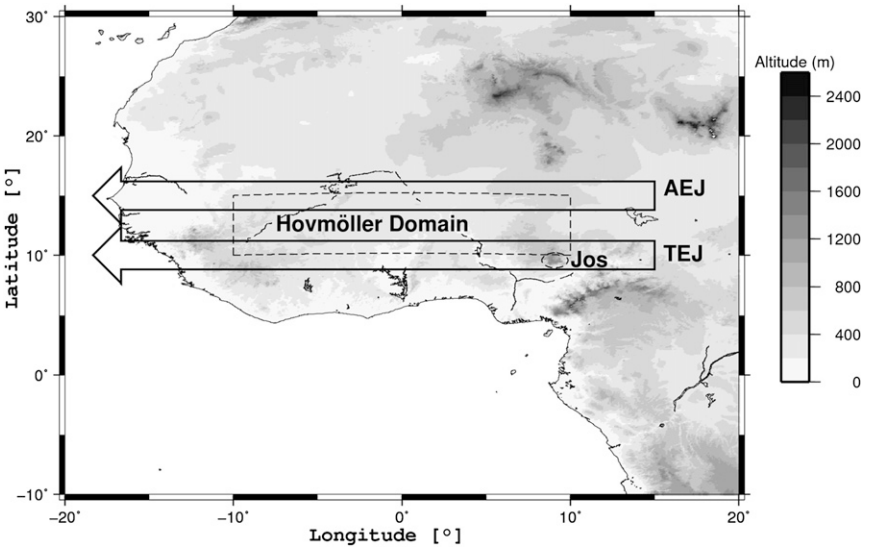

FIG. 1. West Africa with the study area (10°S–30°N, 20°W–20°E) outlined. The gray shading indicates high terrain, and the Jos Plateau is indicated by a dashed ellipsis. Mean locations of TEJ and AEJ are highlighted by arrows. The domain of the systematic study is indicated by a dashed rectangle.

for the intense cases than from the less intense cases. Differences are nonetheless quite small. None of the environmental variables appeared to be clear direct predictors of intense cases. The majority of intense convective systems occurred in the region of baroclinicity with high surface potential temperature and low 700-hPa zonal wind speeds.

Fewer studies have focused on the role of the TEJ (Lavaysse et al. 2006; Fontaine and Janicot 1992; Nicholson 2009). This is not surprising since the TEJ maximum is usually along the Guinea Coast, while most MCSs are much farther north and closer to the AEJ maximum. The TEJ is an upper-tropospheric jet (near 200 hPa) known as the upper branch of a Walker-type cell that originates between the Tibetan Plateau and the Indian Ocean (Krishnamurti and Bhalme 1976; Fontaine and Janicot 1992; Cook 1999). When the monsoon is well developed, the TEJ is over West Africa and is correlated with the monsoon peak, with MCS activity linked to the TEJ. It is split into two speed maxima located on average (decade or monthly means) over Nigeria and Liberia (Reiter 1969; Redelsperger et al. 2002; Diongue et al. 2002; Nicholson and Grist 2003). By using the National Centers for Environmental Prediction–National Center for Atmospheric Research (NCEP–NCAR) reanalysis, National Oceanic and Atmospheric Administration (NOAA) outgoing longwave radiation (OLR), and observed rainfall over West Africa provided by Institut de Recherche pour le Développement (IRD) from 1968 to 1990, Lavaysse et al. (2006) investigated the variability of AEWs, the convective activity, and their relationships with rainfall in wet and dry episodes of the WAM. They showed in particular that during the wet season, the TEJ increases and shifts southward, thus suggesting a strong link between TEJ intensity and convection. Nicholson (2009) examined the factors that modulate the intensity of the rainbelt in the month of August for a wet and a dry year over West Africa. For a wet year, it is shown that the link between the TEJ and rainfall is a causal one, with the strong TEJ enhancing rainfall by enhancing upper-level divergence and sustaining a strong Hadley-type overturning over West Africa with sustained vertical motion.

The main objective of the present study is to analyze how jet streaks and in particular TEJ streaks impact the life cycle of MCSs. This goal will provide new insights, since previous studies have essentially examined the relationship between the AEJ and MCSs (Cornforth et al. 2009; Leroux and Hall 2009; Thorncroft et al. 2007). We will focus on MCSs (linear and shear-perpendicular MCS) but will not consider all types of MCSs (i.e., nonlinear and shear-parallel MCS or isolated convection). This paper makes use of the ageostrophic wind concept used by Uccellini and Johnson (1979) for the midlatitude upper-level jet stream and in numerous studies on the effect of tropospheric jet streaks on severe convective storms (i.e., Petterssen 1956, 191–195; Reiter 1963, see chapters 4 and 6; Ludlam 1963; Newton 1963, 1967; Palmèn and Newton 1969; Danielsen 1974). These studies show the primary role played by the upper-level tropospheric jet streak in advecting cool, dry air in the upper and midtroposphere, in enhancing the upper-level divergence, and in transporting the sensible heat downstream from the convective

region. This ageostrophic concept was also used on African MCSs by Parker et al. (2005), but instead to clarify the role of the AEJ.

In this paper, the ageostrophic concept is first applied to a particular MCS, and then systematically evaluated for a large dataset during the monsoon season 2006 (July and August). In section 2, the description of the data and methods are presented. Section 3 is devoted to the analysis of the case study. A two-month evaluation of MCS activity with mid- and upper-tropospheric jets and associated convergence and divergence is presented in section 4, and concluding remarks are presented in section 5.

2. Data and methods

The primary data used in this study are digitized infrared images at 10.8 μm from the Météosat Second Generation (MSG). These images have a spatial resolution of 5 km $\times$ 5 km at the subsatellite-point (0, 0—the Greenwich meridian–equator intersection), and are available every 15 min. Raw infrared radiation (IR) counts are converted into radiance and brightness temperature T_b using calibration adjustments from the European Organization for the Exploitation of Meteorological Satellites (EUMETSAT; Van de Berg et al. 2003).

MCSs are identified using a cold cloud temperature threshold as done in previous studies of convection in Africa and eastern Atlantic. Duvel (1989) and Machado et al. (1993) used 253 K as a threshold for clouds associated with deep convection. Arnaud et al. (1992) used 233 K to identify clouds that are most likely to produce precipitation. Mathon et al. (2002) found that Sahelian organized systems identified by the 233-K threshold account for 90% of the seasonal rainfall observed by the Etude des Précipitations par Satellite(EPSAT)/Niger rain gauge network over a 9-yr period. Fiolleau and Roca (2013), who developed a method to track MCSs, show the cold cloud shield defined at a 235-K brightness temperature threshold permits the characterization of all the morphological aspects of MCSs during their entire life cycles. For the present study, a 253-K threshold is selected because it allows it to track MCSs all along their life cycles and documents the entire cloud area associated with the deep convection.

The large-scale environment is described using the Interim European Centre for Medium-Range Weather Forecasts (ECMWF) Re-Analysis (ERA-Interim; Dee et al. 2011). These products provide dynamic and thermodynamic fields with a 0.75° grid resolution on 37 isobaric levels at 0000, 0600, 1200, and 1800 UTC each day. As mentioned previously, a case study is presented first for a specific MCS that occurred from 27 to 29 July. For this case study, the domain of interest is 0°–20°N, 20°W–20°E. This case study is meant to define more precisely the relationship between TEJ, AEJ, and the MCS life cycle. Then a more statistical approach is carried out over the monsoon peak of 2006 (July–August) in a domain from 10° to 15°N and 10°W to 10°E (Fig. 1). This latter domain is smaller than the domain used in the case study because it offers, more homogeneous environmental conditions. It is also the region where MCSs contribute the most to the total rainfall, as mentioned in the introduction. To highlight the systematic behavior of this connection between MCSs and the dynamical entities, time–longitude Hovmöller diagrams are constructed. Meridional averages of these fields are performed from 10° to 15°N for every degree of longitude and at each time.

3. Case study

As explained previously, the goal of the case study is to characterize the relationship between a typical African MCS and the TEJ and the AEJ. The selected MCS is particularly well documented by Evaristo et al. (2010) and Scialom and Lemaître (2011) using the Recherche sur les Orages et les Nuages par un Système Associé de Radars Doppler (RONSARD radar; Scialom et al 2009) located at Djougou in Benin during the AMMA special observation period (SOP).

a. *Life cycle*

The MCS is first detected by MSG over the Jos Plateau (Nigeria) at 1300 UTC 27 July (MCS in Fig. 2b), reaches the Atlantic coast above Sierra Leone and Liberia around 1000 UTC 29 July and dissipates over the ocean (Fig. 2d). No MCS activity is observed before initiation over the Jos Plateau, or eastward (MCS in Fig. 2a). The MCS mature stage (MCS in Fig. 2c) occurred approximately over Benin at 0600 UTC 28 July 2006. At that time, the horizontal extent of the system is approximately 660 $\times$ 320 km^2 (using the MSG observation in the visible channel). It is important to note that, during dissipation, the MCS divided into two parts (MCSa and MCSb in Fig. 2d).

During initiation (around 1200 UTC 27 July; Fig. 3), although deep convection has not yet developed, a TEJ core, with wind speed from 20 to 22 m s^{-1}, is located in the southwest region where convective initiation took place in the next hours (see TEJ and MCS in Fig. 3a). A moderately intense (i.e., from 10 to 12 m s^{-1}) AEJ core is present north and east of the system with winds clearly oriented toward the MCS zone (see AEJ in Fig. 3b). Figure 3c shows the divergence field at 200 hPa. In the region of interest (south of 10°N), the divergence field is strongly correlated with the presence of the two TEJ streaks centered at 4°N, 4°E and 6°N, 10°W. The eastern

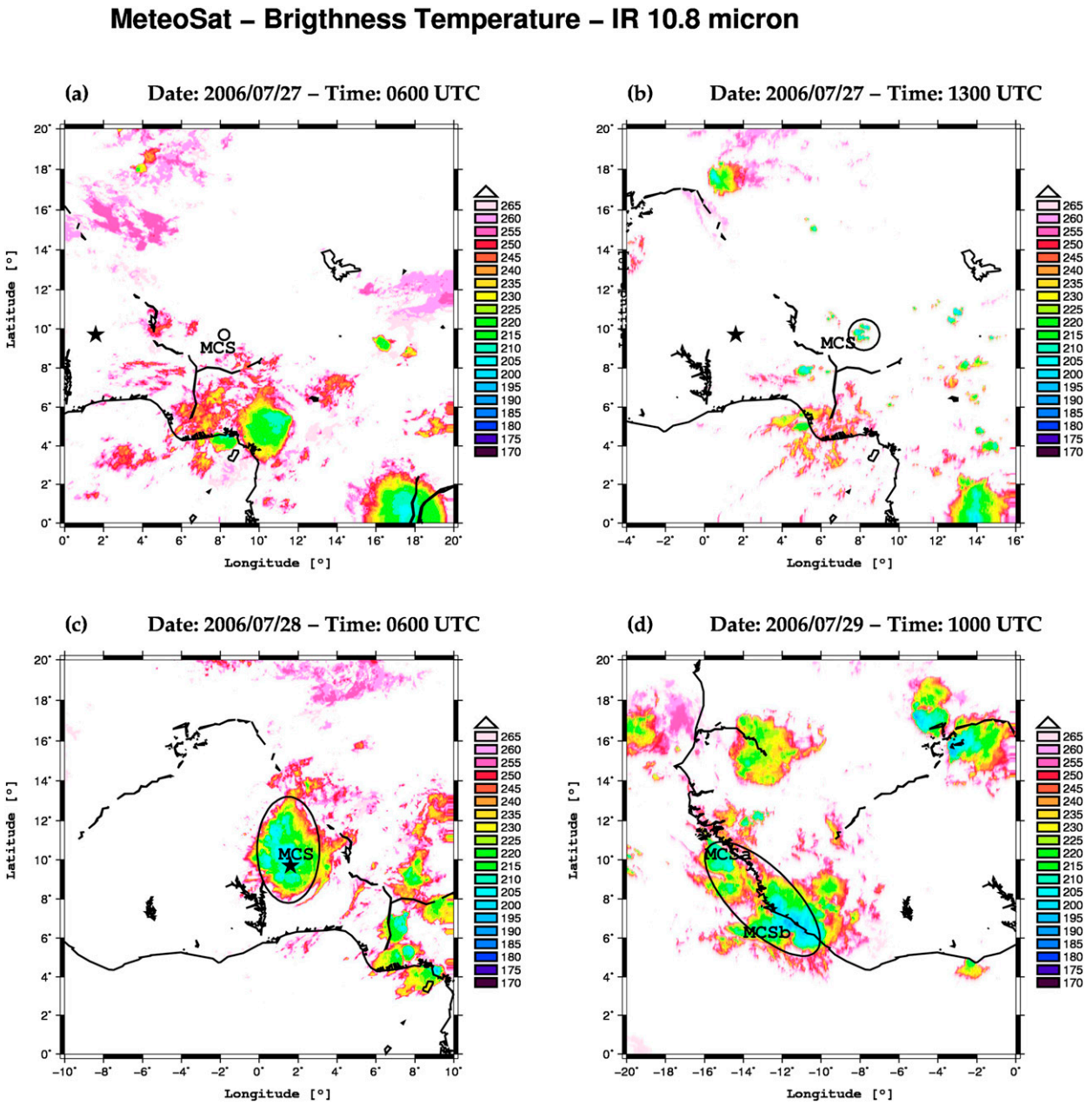

FIG. 2. Brightness temperature images from MSG that give the life cycle of the MCS (a) over the Jos Plateau (Nigeria) at 0600 UTC 27 Jul before initiation (0°–20°N, 0°–20°E), (b) over the Jos Plateau (Nigeria) at 1300 UTC 27 Jul during initiating (0°–20°N, 10°W–10°E), (c) over the Benin at 0600 UTC 28 Jul during mature phase (0°–20°N, 10°W–10°E), and (d) over the Atlantic coast above Sierra Leone and Liberia around 1000 UTC 29 Jul during dissipating (0°–20°N, 20°W–0°). The location of the MCS is indicated by an ellipsis and noted MCS, and the location of the RONSARD radar is indicated by the black star.

streak induces a strong divergence area between 0°–12°N and 4°–10°E. This divergence area has two maxima at 5°N, 8°E and 10°N, 6°E ($\approx 3 \times 10^{-5}\,s^{-1}$). The two maxima are likely to be associated with the TEJ entrance (acceleration zone). It appears much more intense than the monthly mean value typical for August (see, e.g., Nicholson 2009).

Under the classical scheme of geostrophic balance, the wind acceleration associated with the jet streak entrance will induce an ageostrophic response (Uccellini and Johnson 1979) due to the high-level convergence/divergence dipoles, as detailed in section 3b. Figure 3d shows the ageostrophic wind. A southward ageostrophic wind is associated with the streak entrance, a signature

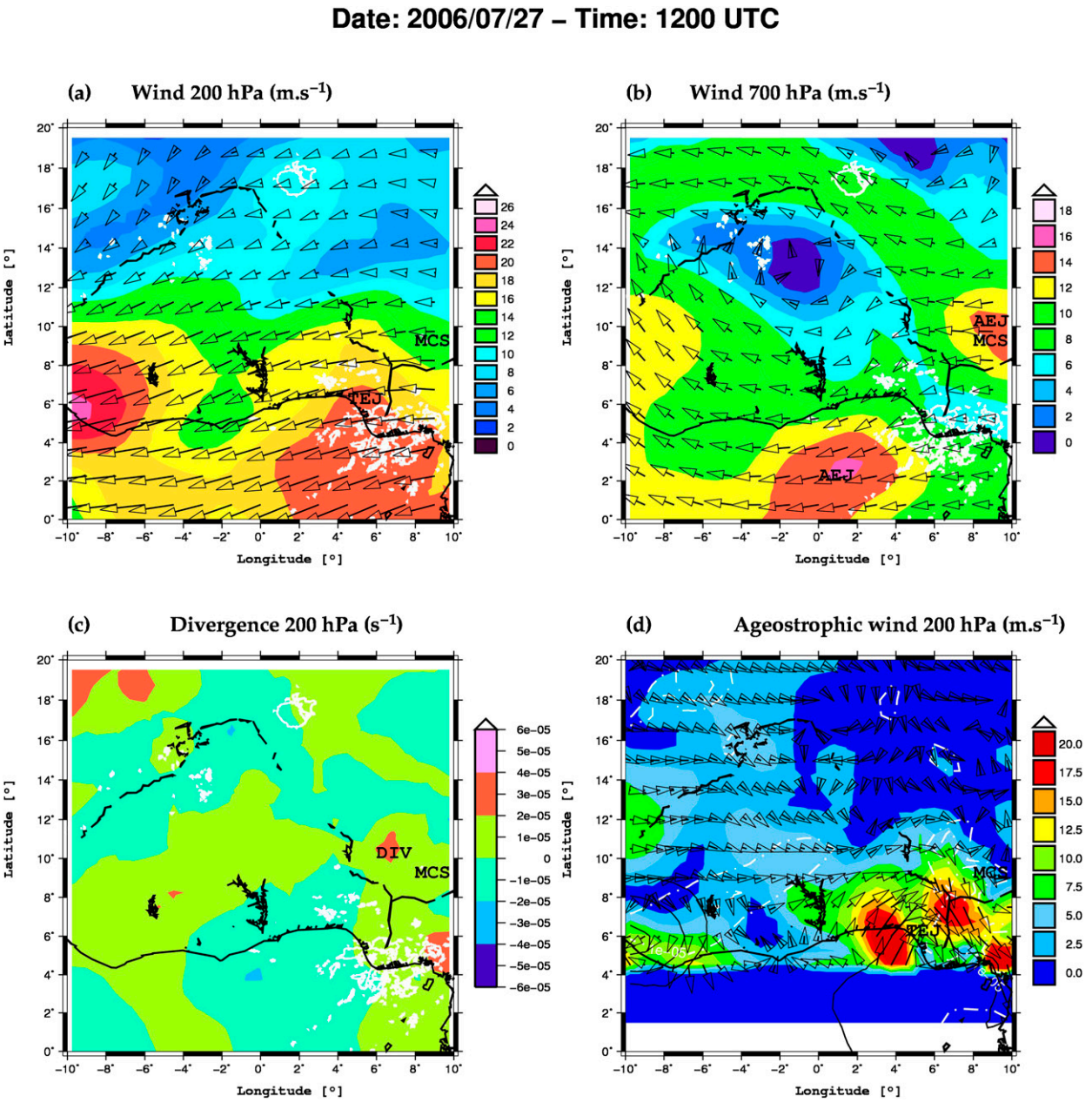

FIG. 3. Horizontal cross section of ECMWF fields at 1200 UTC 27 Jul 2006, the wind speed ($m\,s^{-1}$) (a) at 200 hPa and (b) at 700 hPa, (c) the divergence (s^{-1}) at 200 hPa, and (d) the ageostrophic wind estimation ($m\,s^{-1}$) at 200 hPa. The bold white solid line corresponds to the brightness temperature from MSG (K). The dotted–dashed white line in (d) corresponds to the positive area of divergence. Different dynamic entities are identified by MCS, TEJ, AEJ, and DIV. The thin black line indicates the West African coast and arrows indicate the wind direction. The ageostrophic wind is not calculated below 4° of latitude, since ageostrophic concepts cannot be applied as shown in section 3b.

of the associated counterclockwise transverse circulation as predicted by Uccellini and Johnson (1979). The maximum of divergence observed in the entrance region of the streak (10°N, 6°E) is induced by the ageostrophic acceleration. The second maximum (5°N, 8°E) is related to the TEJ streak acceleration.

The second TEJ streak, located westward, is also in agreement with the theory, a southward-directed ageostrophic wind associated with the streak entrance. We note that the incipient convection is spatially located in the zone of enhanced upper-level divergence. Since the convection is at a very early stage, the upper-level divergence associated with the convection is weak or nonexistent and it is likely that the observed divergence is due mainly to the jet streak.

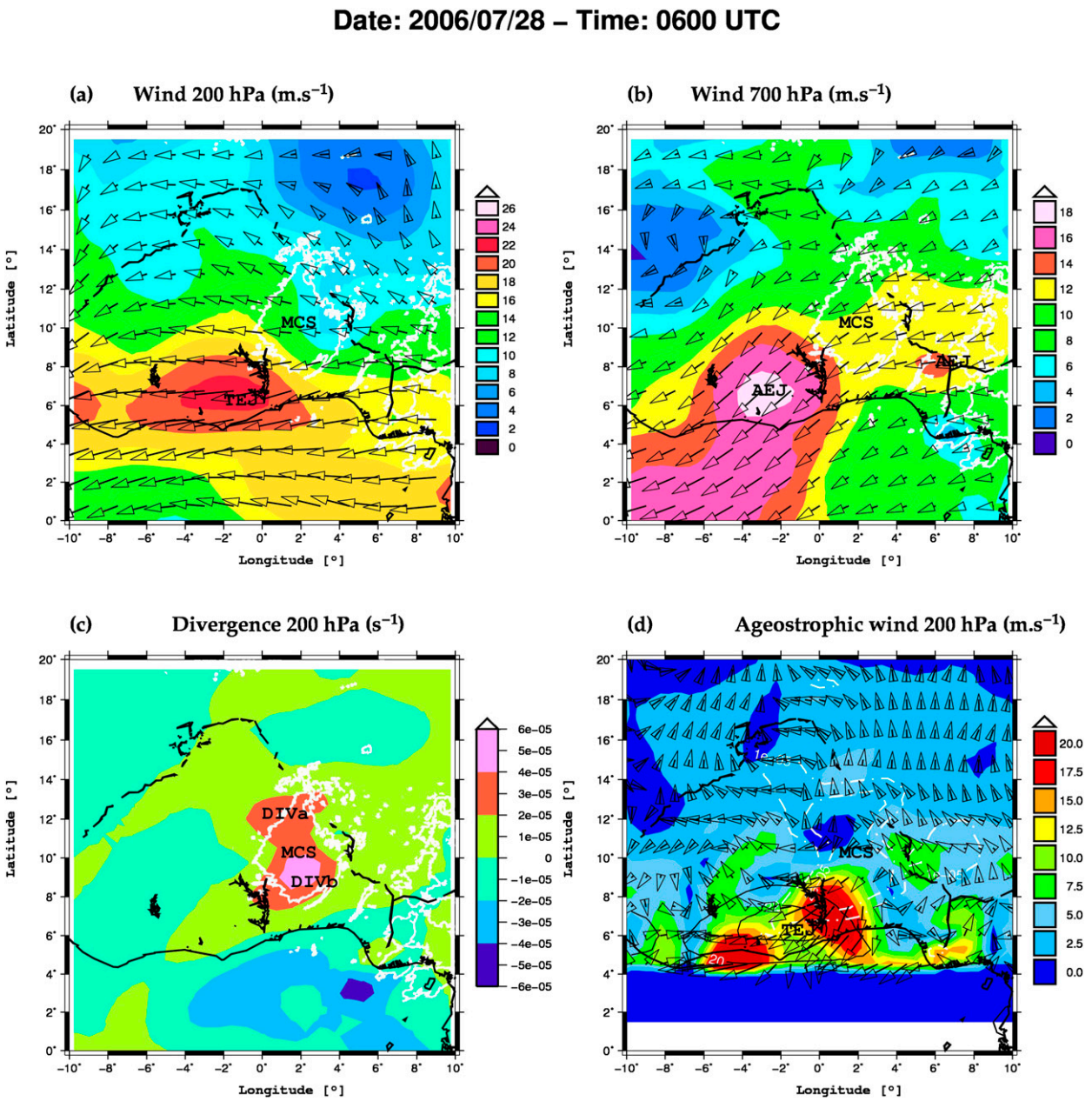

FIG. 4. Horizontal cross section of ECMWF fields at 0600 UTC 28 Jul 2006, the wind speed ($m\,s^{-1}$) (a) at 200 hPa and (b) at 700 hPa, (c) the divergence (s^{-1}) at 200 hPa, and (d) the ageostrophic wind estimation ($m\,s^{-1}$) at 200 hPa. The bold white solid line corresponds to the brightness temperature from MSG (K). The dotted–dashed white line in (d) corresponds to the positive area of divergence. Different dynamic entities are identified by MCS, TEJ, AEJ, and DIV. The thin black line indicates the West African coast and arrows indicate the wind direction. The ageostrophic wind is not calculated below 4° of latitude.

Other processes are known to be critical for convective initiation such as conditional instability, low-level shear, and local dynamic forcing by topography such as the Jos Plateau (Laing and Fritsch 2000; Laing et al. 2008, 2011; Lafore and Moncrieff 1989). For instance, during initiation, the presence of a vertical shear of the horizontal wind (associated in the present case to the AEJ) could inhibit or favor the updrafts (Houze 2004). The AEJ is moderately strong, indirectly favoring the vertical development of the convection, initiated by the divergence area generated by the TEJ streak in the upper troposphere. Also as shown later, the AEJ feeds a rear inflow into the convective system and contributes to the generation of a cold pool cooled by melting and evaporation of hydrometeors. A low-level shear environment should keep the updrafts by counteracting the

negative vorticity of the cold pool (Rotunno et al. 1988). During initiation described above, the MCS appears on the western side of the Jos Plateau.

During the mature phase (around 0600 UTC 28 July; Fig. 4), the convective system is well organized, moving westward with a leading edge and a trailing (stratiform) anvil structure (Evaristo et al. 2010). The TEJ (Fig. 4a) is located on the southwestern side of the convection, and its jet core velocity is now up to 24 m s^{-1}. As shown in Fig. 4d, the direct transverse circulation is now well established with the upward branch associated with an upper-tropospheric divergence (see DIVb in Fig. 4c) maintaining and organizing the MCS (Uccellini and Johnson 1979). This divergence is a combination effect of the ageostrophic direct transverse circulation, the jet acceleration, and the latent heating from the stratiform region. In the northern part of the convective region (see DIVa in Fig. 4c), there is a region of weaker divergence associated with weak ageostrophic winds. This decrease of ageostrophic wind intensity might be due to the increased distance to the TEJ streak entrance. The direct transverse circulation does not influence this part of the MCS.

The AEJ (Fig. 4b) located at the back of the convection (eastern side) is impacting the convective system by supporting the rear inflow as shown by the vertical cross section given in Fig. 5c. This effect influences the life cycle of the convection, through a momentum increase of the gust front strengthening the local convergence, and the propagation of the leading convective part of the system as shown by numerous studies (Lafore and Moncrieff 1989; Diongue et al. 2002; Houze 2004). This link between the AEJ and the cold pool (not totally resolved by the model resolution) is suggested by the observed subsidence of the AEJ at the rear of the updraft region and at low levels (Fig. 5c).

Regarding the TEJ, vertical cross sections taken before and during initiation of the convection (Figs. 5a,b) and during the mature phase (Fig. 5c) suggest a strong dynamical interaction between the TEJ core, the AEJ core, and the convective development. They reveal the presence of vertical motions at upper levels and on the northeastern side of the TEJ core before initiation (see brightness temperatures in Fig. 2a and vertical cross section in Fig. 5a). Then vertical motions at upper levels progressively align with the AEJ exit region during initiation of convective motions located at lower layers (Figs. 2b and 5b). Finally, this leads to a tropospheric column of upward vertical motion during the mature phase of the convective system (Figs. 2c and 5c). As shown in Fig. 5d, the ascending motions observed during the preconvective phase above 4 km are associated with adiabatic cooling indicating that these vertical motions are forced, as latent heating associated with convection results in warming. This cooling is observed down to 4 km indicating that these motions associated with the TEJ affect lower altitudes. These observations tend to confirm an important role of a preexistent upper-level circulation on the development of the convective system.

During dissipation (around 0600 UTC 29 July; Fig. 6), the dynamical environment appears dramatically different. The system splits into two parts. The first one (MCSb in Fig. 6a) is just east of an intense TEJ streak and west of a secondary weaker one. The second (MCSa in Fig. 6) is located north of the more intense TEJ streak within a northward extension of the latter. Jet streak acceleration (deceleration) favors upward (downward) motions as explained previously. Figure 6d illustrates this pattern with weak ageostrophic winds in the MCSa area, and strong ageostrophic winds in the MCSb area. In MCSb, the acceleration induced by jet streak TEJa is much stronger than the deceleration induced by the streak TEJb. Thus, vertical motions associated with TEJa are higher than those induced by TEJb, leading to a high divergence value (DIVb) (Fig. 6c). In contrast, MCSa exists in a poorly defined entrance region, with weak ageostrophic winds and weak upper-level divergence (DIVa) not as favorable as in area DIVb (Fig. 6c).

The northeast–southwest orientation (Fig. 6b) of the AEJ is now perpendicular to propagation of the convective system that decreases the favorable effect of the inflow at the rear of the system. The decrease in the AEJ contribution to the rear inflow slows the MCS down. It also leads to a decrease in the environmental shear. This would lead to less tilted updrafts, which make it hard to maintain an intense inflow and a separation between warmer rising air and precipitation. Warm and moist low-level air cannot be brought in fast enough to form new convective cells. The convective system is now motionless. Moreover, because TEJ and AEJ jet cores are still moving to the west, their favorable impact (in terms of ageostrophic winds and shear) on the convection decreases progressively with the distance between the jet core and the convection.

Moreover, the synoptic-scale flow that initially creates a favorable environment for the formation of this large convective system, through the production of convective available potential energy (CAPE) by horizontal advection and the enhancement of low-level convergence in the region where the convective system formed (see, e.g., Protat and Lemaître 2001), disappears. As the system propagates into an unfavorable environment with limited conditional instability, it progressively dissipates.

b. *Conceptual pattern*

The different observations made in section 3a suggest a favorable spatial pattern of dynamic entities in the

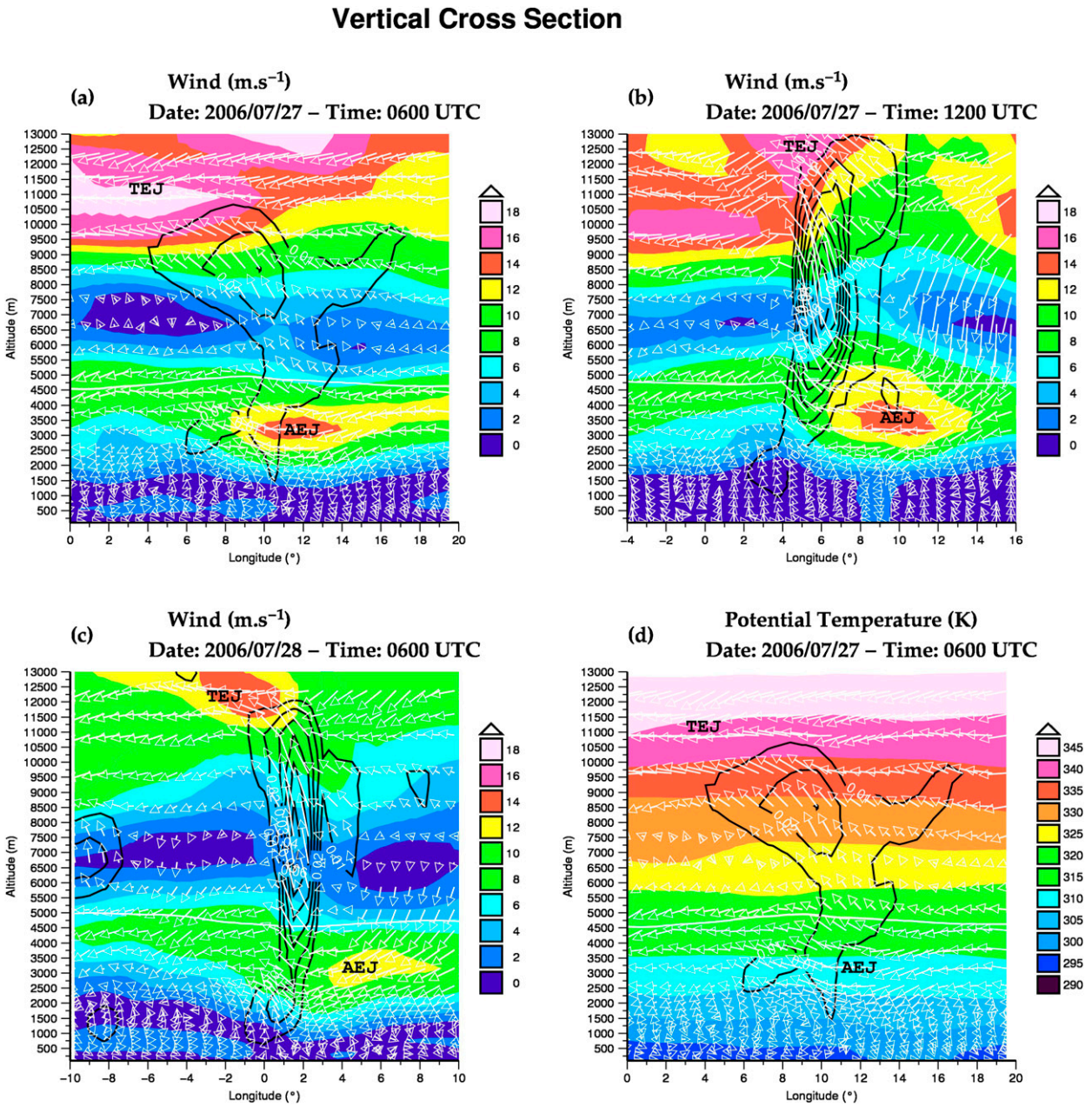

FIG. 5. Vertical cross section of the horizontal wind speed at (a) 0600 UTC 27 Jul 2006 at 8.5°N, (b) 1200 UTC 27 Jul 2006 at 9.25°N, and (c) 0600 UTC 28 Jul 2006 at 10.5°N, and (d) the vertical cross section of the potential temperature (K) at 0600 UTC 27 Jul 2006 before initiating. Cross sections are depicted on the northeastern side of the TEJ, between 10°W and 10°E. Different dynamic entities are identified by TEJ and AEJ. The thin white line indicates the 0-K temperature isotherm, the color pattern corresponds to the horizontal wind speed ($m\,s^{-1}$), white arrows indicate the wind orientation, and black contours indicate positive vertical motions ($m\,s^{-1}$).

vicinity of MCS. In particular, the TEJ and AEJ seem to directly impact the convection through the development of a divergence area at the top of the troposphere and the enhancement of the rear inflow. A conceptualization of this particular configuration promoting convective systems is given in Fig. 7a. First, the convective system is located on the north side of the intense TEJ wind core (Figs. 3a and 4a). Second, the AEJ streak is located behind the cloud systems (Figs. 3b and 4b). Thus, two different and complementary interpretations of this particular pattern are considered. These interpretations rely on two different physical processes in order to explain the location of the convective cells relative to the TEJ. The first one is based on the classical concepts of

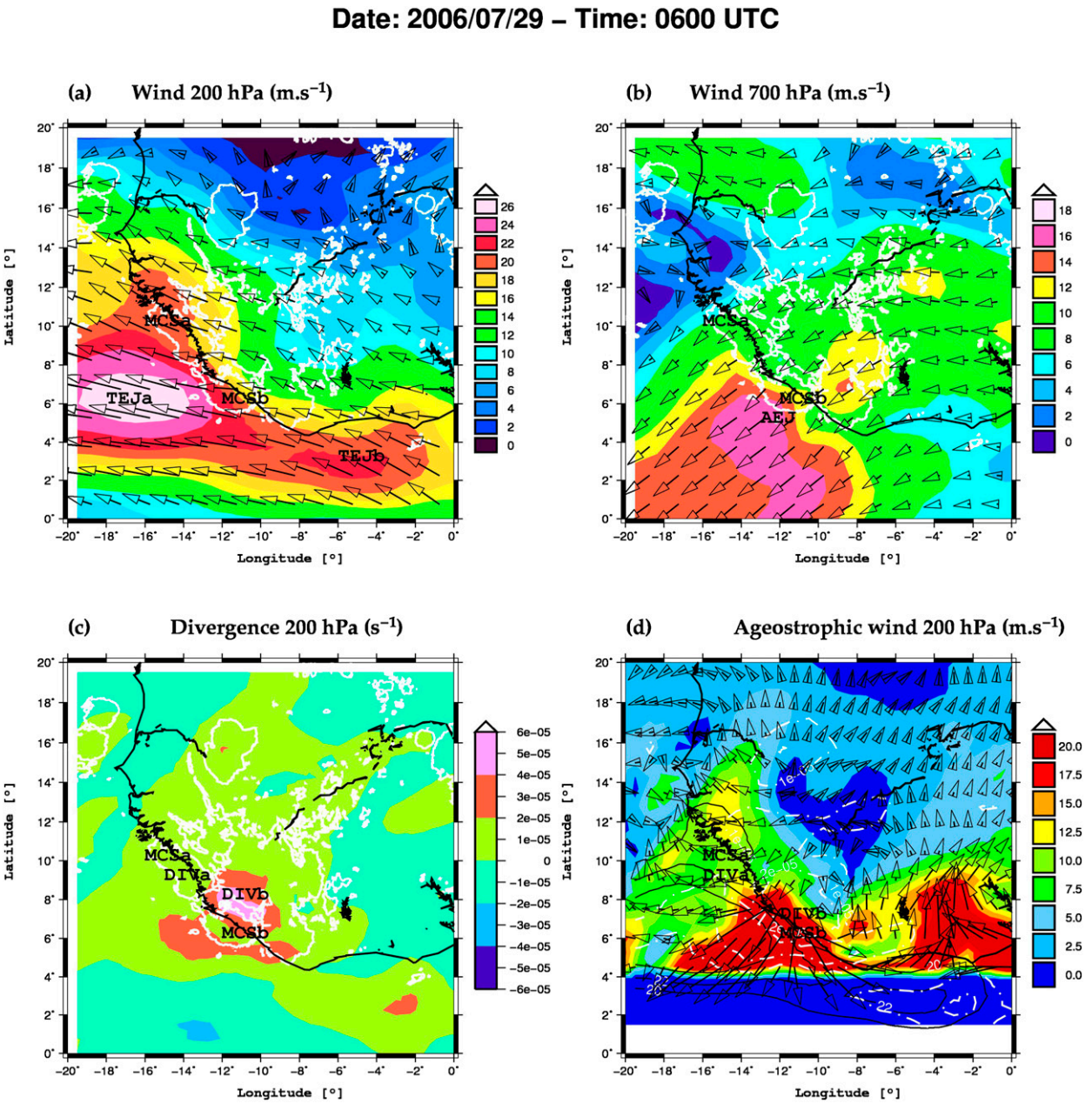

FIG. 6. Horizontal cross section of ECMWF fields at 0600 UTC 29 Jul 2006, the wind speed ($m\,s^{-1}$) (a) at 200 hPa and (b) at 700 hPa, (c) the divergence (s^{-1}) at 200 hPa, and (d) the ageostrophic wind estimation ($m\,s^{-1}$) at 200 hPa. The bold white solid line corresponds to the brightness temperature from MSG (K). The dotted–dashed white line in (d) corresponds to the positive area of divergence. Different dynamic entities are identified by MCS, TEJ, AEJ, and DIV. The thin black line indicates the West African coast and arrows indicate the wind direction. The ageostrophic wind is not calculated below 4° of latitude.

divergence and convergence, in entrance/exit regions of the upper-level jet streaks. In entrance regions, the wind acceleration creates a divergence area that, since the jet is located at the top of the troposphere, could promote ascending motions on the entire of the column depending on the stability. In the opposite way, in exit regions, where the wind is decelerating and creates a convergence zone, downward motions are favored. Thus, upward motions are promoted to the east of the jet streak and their intensity is partly controlled by the wind acceleration determined by the strength of the jet core.

A rough estimate of vertical motions produced by such accelerations can be done for the previous case study (28 July 2006). The divergence in the entrance region of the

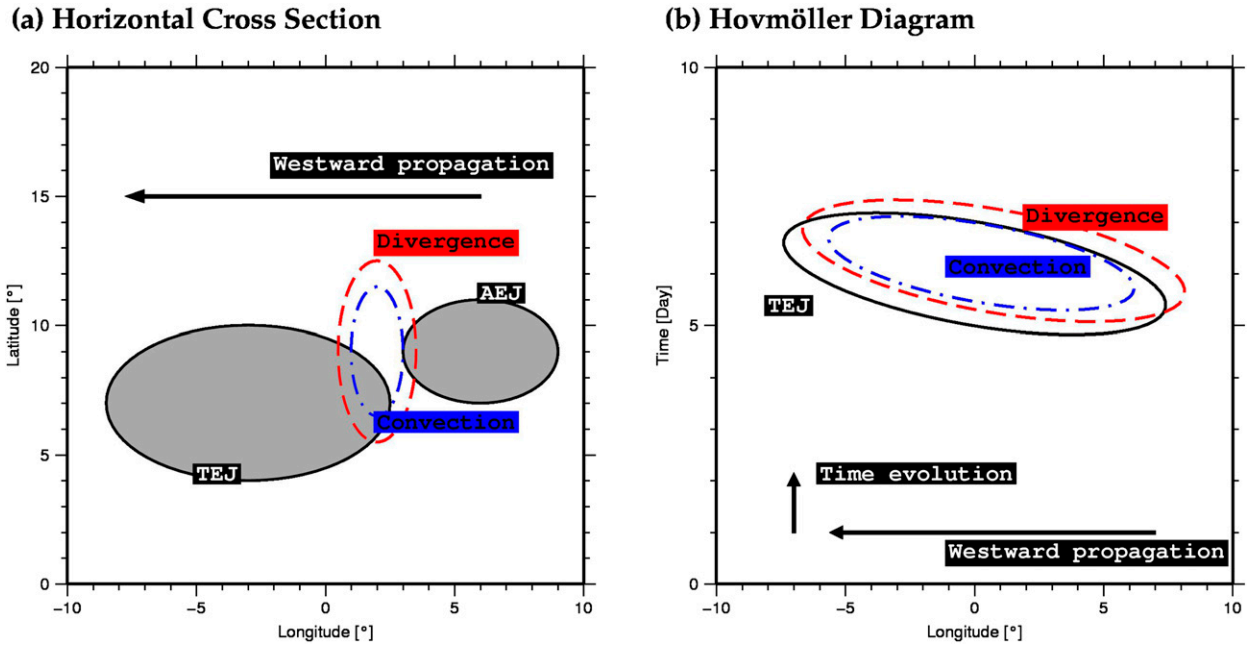

FIG. 7. Illustration of (a) the conceptual pattern expected for the spatial configuration between the TEJ, the divergence area, and the convection. The convection is ahead of the AEJ, northeastward of a strong TEJ wind core. The dynamic complex results in a westward displacement. (b) The corresponding pattern for a time–longitude Hovmöller diagram.

upper-level jet streak is around $3 \times 10^{-5}\,s^{-1}$ (Fig. 4c). Integrating downward the continuity equation from the top (100 hPa) and until 200 hPa with this divergence value, assuming the vertical velocity to be null at the tropopause, leads to a vertical wind speed of $0.12\,m\,s^{-1}$ at 200 hPa. The vertical wind from ECMWF ($0.8\,m\,s^{-1}$) supports the dynamical impact of the TEJ streak for this case.

The second interpretation is based on the concept of ageostrophic wind. In this concept vertical motions are required to maintain the thermal wind balance in response to a large-scale forcing such as frontogenesis, upper-level waves, or jet streak phenomena. This secondary circulation has been the object of numerous studies for midlatitude systems (Namias and Clapp 1949; Uccellini and Johnson 1979; Hoskins et al. 1985; Thorpe and Emanuel 1985; Brill et al. 1985; Uccellini and Kocin 1987; Xu 1989; Huang and Emanuel 1991; Lagouvardos et al. 1992; Lemaître et al. 1994). The concept predicts that in the entrance region of upper-level streaks, in the Northern Hemisphere the wind is diverted to the left by a horizontal ageostrophic component superimposed on the geostrophic wind (e.g., Uccellini and Johnson 1979). This ageostrophic component generates a direct transverse circulation, with a divergence area on the right-hand side, and a convergence area on the left-hand side of the streak entrances. In the exit regions of the streaks, an indirect circulation is observed with a convergence area on the right and a divergence on the left.

Thus, favorable regions for convection are also expected in the northern side of the entrance region of the upper-level jet core. The intensity of the convergence and divergence zones is controlled by the intensity of the ageostrophic wind that is related to the temporal variation (Lagrangian) of the total wind. For tropical regions, Parker et al. (2005) have shown that the AEJ is close to the thermal-wind balance, supporting the potential use of such concepts. For the TEJ, a rough estimate of the Rossby number (V/Lf) can be done. The typical value of the zonal wind speed V ($20\,m\,s^{-1}$), the typical length scale of the jet L (from 1500 to 2500 km), and the Coriolis parameter f ($1.996\,63 \times 10^{-5}$ at 7.875°N) give a value between 0.66 and 0.4 for the Rossby number. As result of the Rossby number being lower than 1 for the latitudes greater than 8°N, for these regions the ageostrophic concept can be used as a first approximation for the TEJ.

Without the geostrophic balance, the jet streak should produce a two-cell pattern of divergence and convergence associated with the entrance and exit regions of the jet, respectively. In presence of geostrophic balance, the straight jet streak should lead to a four-cell pattern of convergence and divergence as described by Uccellini and Johnson (1979) and Moore and VanKnowe (1992). The solution depends on the local value of the Rossby number. A high value when the Coriolis force is weak should support the two-cell pattern and a low value

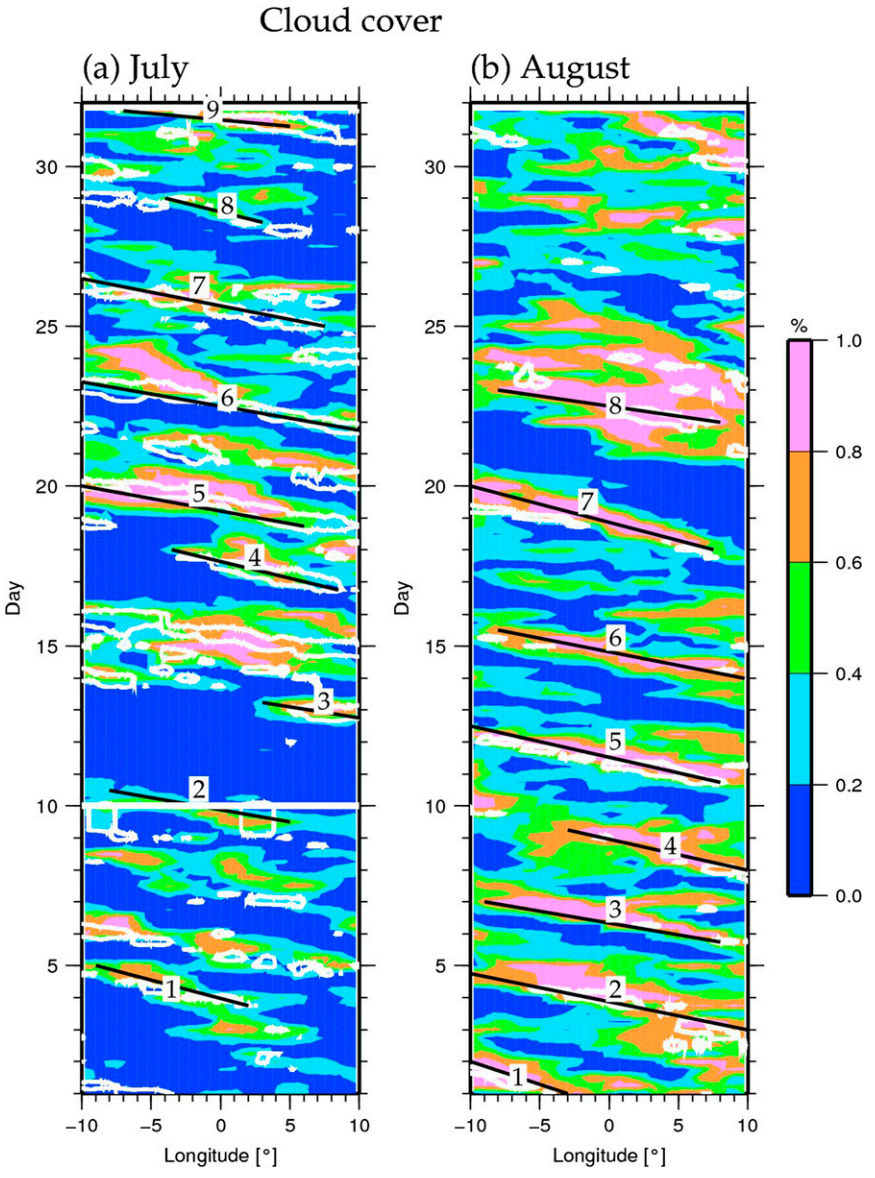

FIG. 8. Hovmöller diagrams on the high cloud cover from ECMWF (in color field) for (a) July and (b) August, averaged between 10° and 15°N (for July). The brightness temperature from MSG (253-K threshold) is indicated by the white contour. Solid white lines indicate the onset of the monsoon season. The solid black line corresponds to MCSs trajectories.

when TEJ winds are light or when the Coriolis force increases, favors the four-cell pattern. An intermediate value will not completely support the four-cell pattern and a hybridation of the two mechanisms would take place. The resulting divergence areas are located more or less on the right-hand side of the jet core, more or less at its rear. The location of the divergence maximum is highly dependent of the contribution of each of the different processes. Note that the exit region of the jet streak is no longer a favorable configuration to support convective motion since in this region the divergence due the ageostrophic circulation located on the southern side of the exit region is now superimposed onto the convergence zone produced by the jet deceleration.

4. Systematic study

In this section, the conceptual representation of the dynamic environment of areas favorable for the African convection is evaluated for the active monsoon period (July and August) of AMMA using the Hovmöller representation described in section 2. In this Hovmöller

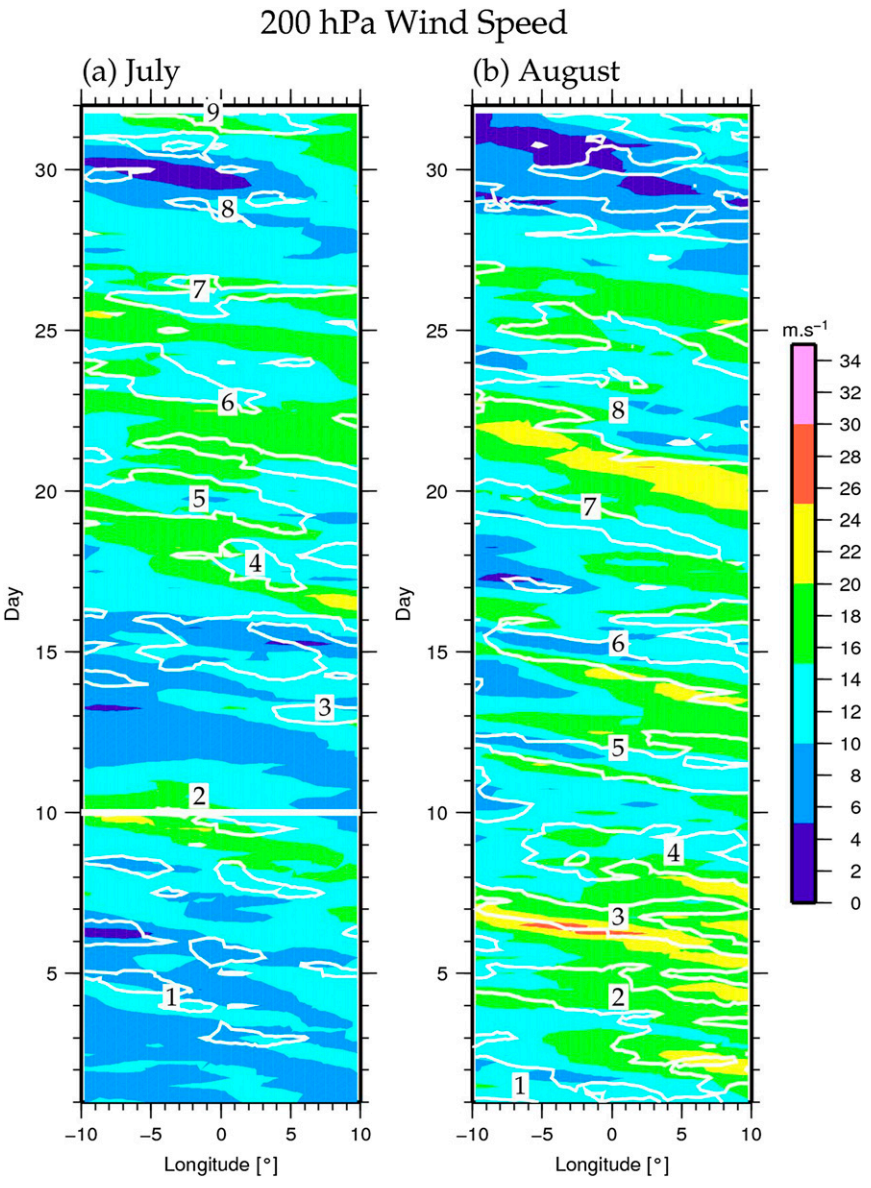

FIG. 9. Hovmöller diagrams on the wind speed at 200 hPa from ECMWF for (a) July and (b) August, averaged between 10° and 15°N. The high cloud cover from ECMWF is indicated by white contours. The white solid line represents the onset of the monsoon season. Numbers inside the cloud contour indicate the well-reproduced cloud systems observed by MSG in the ERA-Interim.

representation, the divergence area induced by the TEJ should be slightly shifted backward of the jet streak in time or in longitude. The convection is most likely to be located in the divergence area.

We evaluated ECMWF products before using them to investigate the systematic relationship between convective systems observed during the AMMA experiment and their environment. The high cloud cover (HCC) fields from ECMWF are evaluated against the 10.8-μm brightness temperatures T_b from MSG observations. Although the correlation between the brightness temperature and HCC in West Africa and the ability of ECMWF operational models to reproduce the gross features of the monsoon is well known (e.g., Mounier et al. 2007, 2008; Mathon and Laurent 2001; Mathon et al. 2002; and ECMWF model verification studies), it is interesting to perform a specific comparison for the present dataset.

Figures 8a and 8b show this comparison for July and August provided by the ERA-Interim and by MSG (using the 253-K threshold, white contour), respectively.

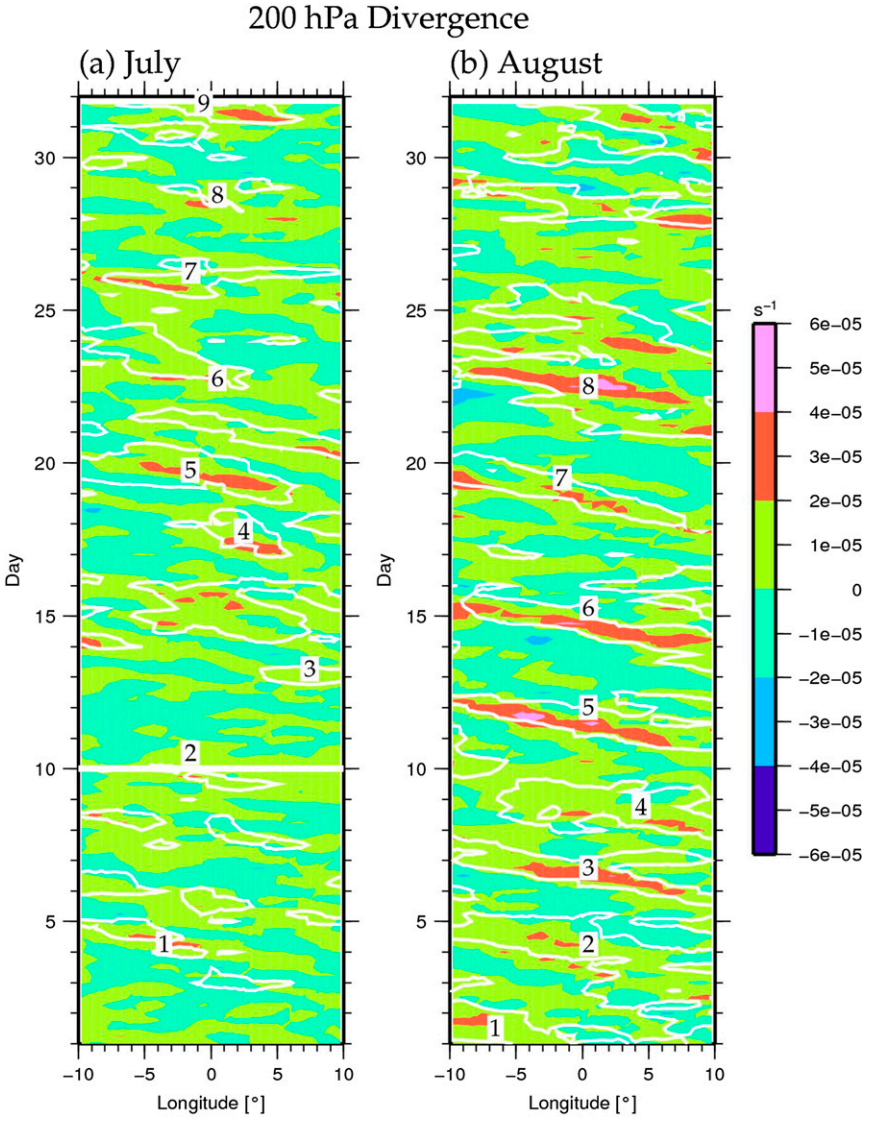

FIG. 10. Hovmöller diagrams of the divergence at 200 hPa from ECMWF for (a) July and (b) August, averaged between 10° and 15°N (for July). The high cloud cover from ECMWF is indicated by white contours. The white solid line represents the onset of the monsoon season. Numbers inside the cloud contour indicate the well-reproduced cloud systems observed by MSG in the ERA-Interim.

They show a relatively good agreement between low T_b and HCC values, with a quasi collocation of the T_b and of the high cloud. It also shows an agreement between the time evolution and longitude motion of the T_b patterns and of the HCC. This indicates that the ECMWF ERA-Interim provides a relatively good representation of the monsoon thermodynamics. In the following study, we use the cloud information provided by the ERA-Interim. This choice will maintain the internal coherence between MCSs and environmental conditions (dynamic/thermodynamic) given by the ERA-Interim.

Results of Hovmöller diagrams are given in Figs. 9a and 9b for July and August, respectively. First, convective systems, well reproduced in the ERA-Interim indicated by white contours and numbers in Figs. 9a,b (giving cloud tracks), appear clearly related to intense TEJ periods suggesting that the TEJ streaks can promote MCSs. These observations confirm previous studies done by Druyan and Hall (1996), Thorncroft and Blackburn (1999), Redelsperger et al. (2002), and Nicholson and Grist (2003). Figures 9a,b also confirm that cloud systems appear after a TEJ maximum with a slight time delay (see, e.g., cases 2, 4, and 5 in July; Fig. 9a), or

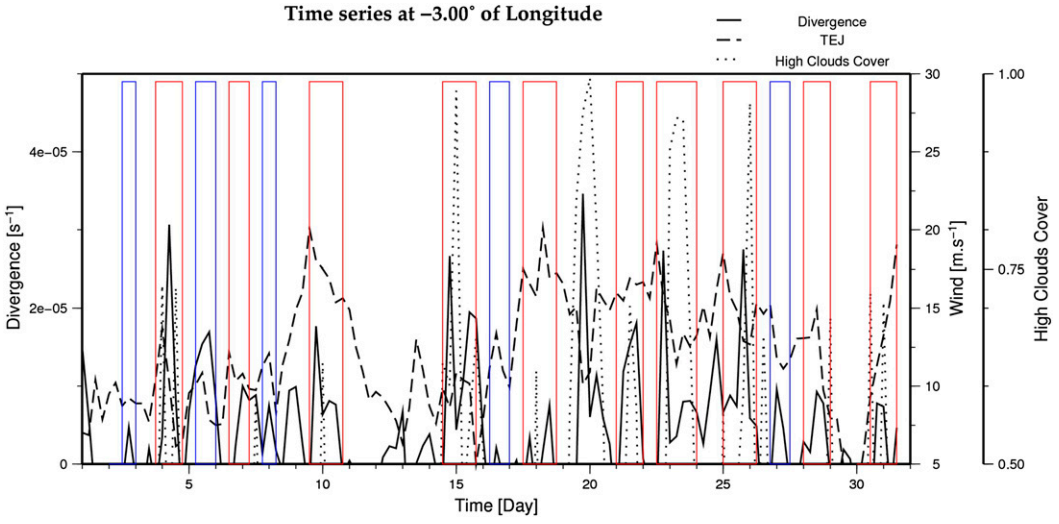

FIG. 11. July's time series of the wind speed (dashed line) and divergence (solid line), both at 200 hPa, and the high cloud cover (HCC, dotted line) at 3°W. Rectangles indicate the time period when there is divergence associated with the TEJ. The red color corresponds to convective activity and the blue color corresponds to a lack of convection.

eastward of the jet streak (see, e.g., cases 3 and 6 in August; Fig. 9b). For case 4 in August, the time lag between the maximum and the convective system along the 2° longitudinal line is 6 h (i.e., the used minimum time resolution provided by the ECMWF dataset). Similarly for case 7 in August, a spatial shift in longitude of about 1° is observed. These two configurations show that the convective system is located eastward of the TEJ wind core.

As shown by the conceptual model discussed in section 3b, this more or less systematic TEJ location ahead of the convection results partly from the fact that the TEJ streak is a source of upward motion at upper levels through the induced divergence area. To confirm this interpretation it is necessary to analyze the divergence field at 200 hPa (Figs. 10a,b). It can be noted that convective systems form preferentially in areas of upper-tropospheric divergence. The maximum of divergence

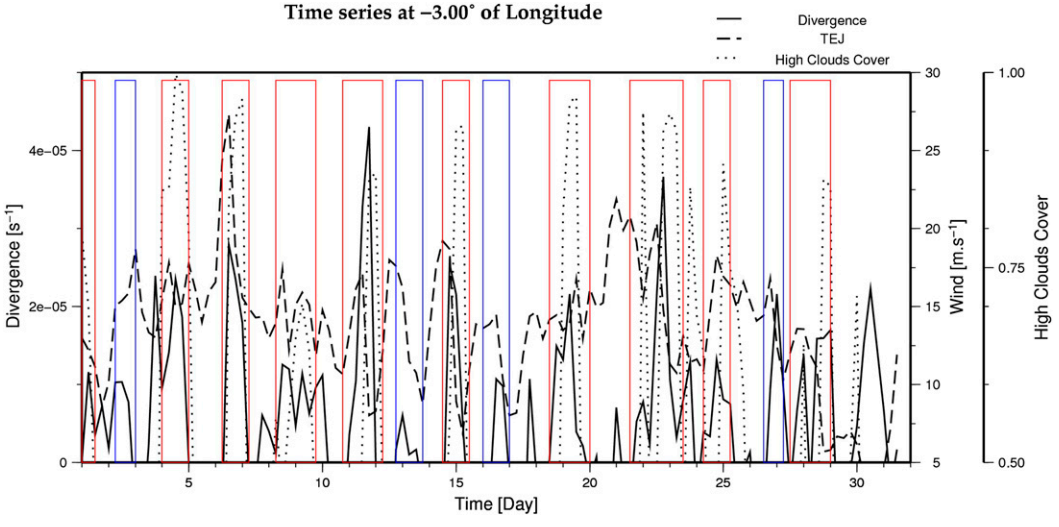

FIG. 12. August's time series of the wind speed (dashed line) and divergence (solid line), both at 200 hPa, and the high cloud cover (HCC, dotted line) at 3°W. Rectangles indicate the time period when there is divergence associated with the TEJ. The red color corresponds to convective activity and the blue color corresponds to a lack of convection.

TABLE 1. Correlation coefficient calculated for July and August between cloud cover observed vs wind core maximum and divergence as a function of time lag.

	Wind			Divergence		
	t (0 h)	$t-6$ h	$t-12$ h	t (0 h)	$t-6$ h	$t-12$ h
HCC t (0 h)	−0.04	0.13	0.35	0.18	0.45	0.12

TABLE 2. Correlation coefficient calculated for July and August between wind core vs divergence as a function of time lag.

		Wind		
		t (0 h)	$t-6$ h	$t-12$ h
Divergence	t (0 h)	0.07	0.30	0.17
	$t-6$ h		0.0029	0.34
	$t-12$ h			0.07

occurs during the maximum of MCSs occurrence, confirming that organized convection contributes to upper-tropospheric divergence area via latent heating. However, before or during initiation of the convective systems, when the convection does not yet impact the upper levels, divergence is observed in the area of future convective systems (see situation noted by numbers in Figs. 10a,b, where along constant longitude, divergence appears before the cloud maximum). The divergence area appears larger than the area of convection. Those observations show a good agreement with the proposed conceptual pattern.

To confirm the effect of the TEJ on MCSs, the time evolution of the TEJ speed, the divergence at 200 hPa, and the HCC intensity averaged from 10° to 15°N at 3°W are constructed for July and August and given in Figs. 11 and 12, respectively. Most of the time (red rectangles, Figs. 11 and 12), the TEJ jet core is observed before the divergence area, associated with system development. It can be noted that divergence areas are not necessarily correlated with the development of an MCS (blue rectangles, Figs. 11 and 12). The upper-tropospheric diffluence associated with the TEJ produces a favorable environment for MCS organization and development but is subject to constraints on convective initiation imposed by conditions at lower levels.

To evaluate the contribution of the TEJ on the convection, correlation coefficients between the wind velocity, the divergence, and the HCC are calculated from this time series. In this calculation, time lags have to be taken into account and are arbitrarily chosen and imposed by the time resolution of the ECMWF dataset (i.e., 6 h). Because the initiation and development of MCSs require multiple processes at different scales and at different levels of the troposphere, correlation coefficients can be expected to be low. However, correlation maximum will give a rough estimate of the time lags between the three entities. To limit the contribution of other atmospheric mechanisms, such as the diurnal cycle, time lags larger than 12 h between the wind core and the convective activity are disregarded.

Table 1 contains correlation coefficients for different time lags between MCSs (at time 0), wind core, and divergence occurrence. As expected, correlations are better when accounting for time lags than without. For a convective event observed at time 0, the highest correlation with wind core and divergence are for a TEJ that occurs 12 h before ($R = 0.35$) and a divergence maximum that occurs 6 h ($R = 0.45$) before the convection.

The relationship between the wind core and the divergence is more complex. The highest correlation is obtained for a jet core that occurs 12 h before the convection and 6 h before the divergence ($R = 0.34$ in Table 2). The correlation between the wind core 6 h prior to convection and the divergence at the time of convection is also higher ($R = 0.30$). These correlations appear rather low. This indicates that upper-tropospheric processes enhancing system development and maintenance do not dominate lower-tropospheric processes controlling convective initiation and intensity such as CAPE and environmental shear. Note that the correlation coefficients change with the time lags. There would be no change if there were not clear benefits to systems development from upper-level divergence associated with TEJ streaks. Note also that the time resolution of the analysis strongly constrains the correlation calculation. It does not allow us to infer intermediate time lags that could increase the resulting correlation coefficients. From these correlations, it can be concluded that time delays of 12 h between the wind core and the system, and 6 h between the divergence occurrence and the system are observed. This chain of association is observed for other longitude (not shown) and cases selected previously.

The connection between MCSs and the AEJ appears more complex. Convective systems appear mostly ahead of the AEJ jet streak (e.g., cases 3, 5, and 6 in July; Fig. 13a and cases 5 and 6 in August; Fig. 13b) and the growth of deep convection appears highly dependent on the jet intensity. A high jet velocity seems to inhibit convective development (see the period from 16 to 17 July between 5° and 10°W), and a weak jet leads to nonpropagating convective systems (see the period from 29 to 31 July) and therefore short-lived systems. These observations are in agreement with previous studies (e.g., Adedoyin 1989; Hodges 1998), which found that an intensification of the AEJ plays a role in the maintenance and the generation of new convective cells but prevents any local development in the absence of preexisting convection. Other processes have to be taken into account

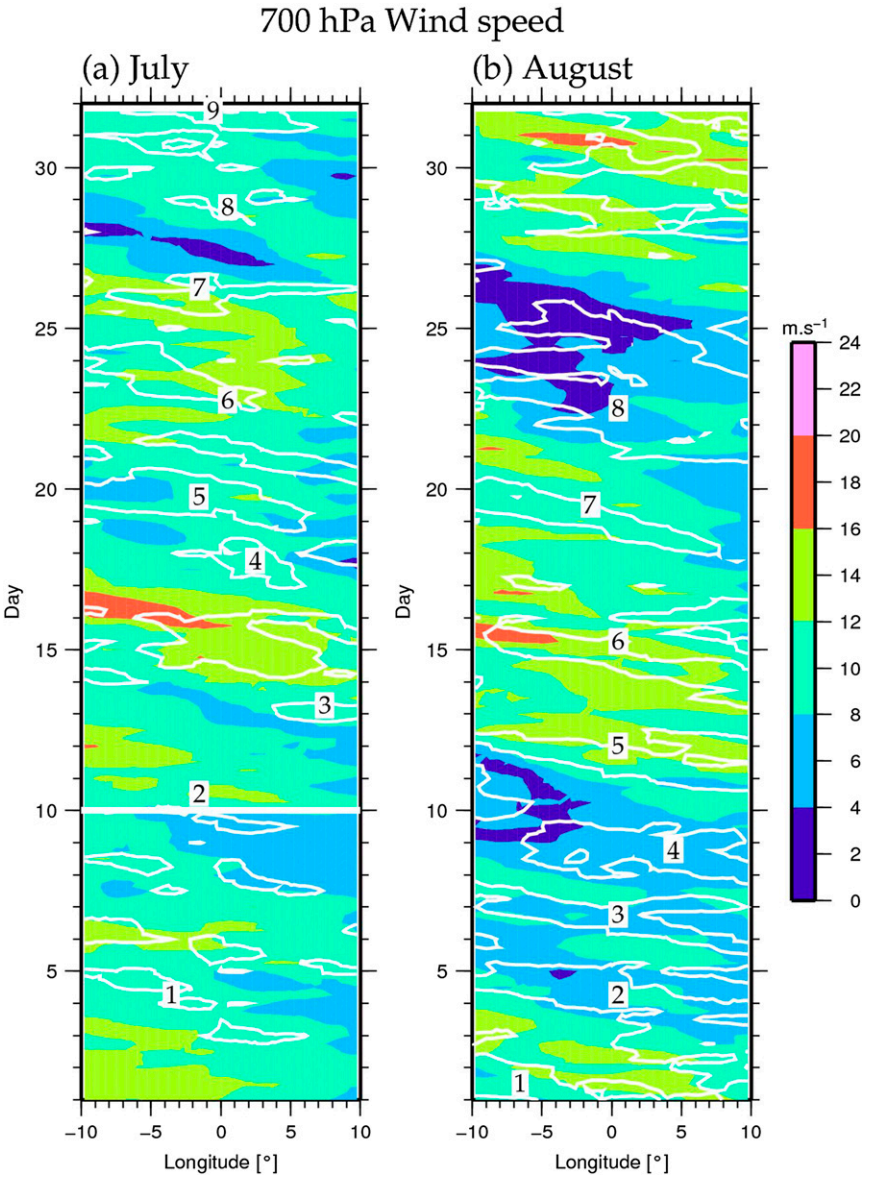

FIG. 13. Hovmöller diagrams of the wind speed at 700 hPa from ECMWF for (a) July and (b) August is averaged between 12.5° and 15°N (for July). The HCC from ECMWF is indicated by the white contour. The solid white line indicates the onset of the monsoon season. Numbers inside the cloud contour indicates the well-reproduced cloud systems observed by MSG in the ERA-Interim.

such as the wind shear that also impacts the propagation speed of cloud systems (e.g., Adedoyin 1989; Hodges 1998; Laing et al. 2008). This location of the AEJ to the east of the cloud systems that can promote the generation and the maintenance of the mesoscale rear inflow is shown to have an important effect on the convective region. It enhances the low-level convergence and the mass flux in the cold pool (i.e., Lemaître 1982; Lemaître and Testud 1986; Moncrieff and Klinker 1997; Houze 2004; see also the case study described in section 3a).

5. Conclusions and perspectives

This study makes use of theoretical concepts (ageostrophic winds) initially developed for midlatitudes (Uccellini and Johnson 1979; Uccellini and Kocin 1987; Cammas and Ramond 1989) and uses them to characterize the interaction of the TEJ and AEJ with MCSs. The case study and the systematic study show that convective systems over West Africa seem to maintain a close relation with the AEJ and TEJ. A favorable

pattern between these entities for intense and long-lived systems is identified and described. The most favorable location for long-lived systems is in the entrance region of the TEJ streak characterized by an upper-tropospheric divergence area, combining the effect of the ageostrophic circulation and of the jet acceleration. The jet diffluence allows for the ventilation of the latent heating associated with convective clouds. The intensity of the forcing is directly linked to the jet streak and the maintenance of the phasing between convection and jet that favors long-lived systems. The cloud systems are also generally located in front of an AEJ core. This jet is essential in feeding the mesoscale inflow at the rear of the mesoscale convective systems that partly controls the convective region by enhancing the low-level convergence and the mass flux in the cold pool.

This dynamic configuration between TEJ, AEJ, and convection favorable for large, fast, and well-organized convective systems seems to be confirmed by the present dataset. However, this favorable configuration is strongly sensitive to any modification of the synoptic situation, such as a phase shift between these three entities due to their relative motions, that can led to the dissipation of the MCS. This dynamic configuration appears important to explain the life cycle of the MCS. While convective initiation is controlled by the local dynamical forcing and CAPE, the system organization and development is affected by the spatial and temporal variability of the TEJ and AEJ.

These results raise several questions for which it will be necessary to perform further studies. The main question concerns the processes of coupling between the convection (and the associated latent heating) and these dynamic entities that induce the observed phasing for long-lived MCSs. Can it be treated, as in the case of midlatitude systems, in terms of response using quasi- and semigeostrophic backgrounds? Can the propagation of the system be explained in this framework, too? Such questions could be scrutinized using multiples datasets from observations or mesoscale and large-scale numerical models and the Analyse du Vent Agéostrophique (AVAG) analysis (Lemaître et al. 1994) in order to document the ageostrophic circulations and associated latent heating effect from wind and temperature fields.

Acknowledgments. Based on a French initiative, AMMA was built by an international scientific group and is currently funded by a large number of agencies, particularly from France, the United Kingdom, the United States, and Africa. It has been the beneficiary of a major financial contribution from the European Community's Sixth Framework Research Programme. Detailed information on scientific coordination and funding is available on the AMMA International website (http://www.amma-international.org). Special recognition must be made to Drs. Nicolas Viltard and Georges Scialom for their helpful comments. Moreover, the authors wish to thank the reviewers for their constructive comments and for helping with the English correction.

REFERENCES

Acheampong, P. K., 1982: Rainfall anomaly along the coast of Ghana—Its nature and causes. *Geogr. Ann.,* **64A,** 199–211.

Adedoyin, J. A., 1989: Initiation of West African squall lines. *Meteor. Atmos. Phys.,* **41,** 99–103, doi:10.1007/BF01043455.

Arnaud, Y., M. Desbois, and J. Maizi, 1992: Automatic tracking and characterization of African convective systems on Meteosat pictures. *J. Appl. Meteor.,* **31,** 443–453, doi:10.1175/1520-0450(1992)031<0443:ATACOA>2.0.CO;2.

Bayo Omotosho, J., 1984: Spatial and seasonal variations of line squalls over West Africa. *Arch. Meteor. Geophys. Bioklimatol.,* **33,** 143–150, doi:10.1007/BF02257721.

——, 1985: The separate contributions of squalls, thunderstorms, and the monsoon to the total rainfall in Nigeria. *J. Climatol.,* **5,** 543–552, doi:10.1002/joc.3370050507.

Bolton, D., 1984: Generation and propagation of African squall lines. *Quart. J. Roy. Meteor. Soc.,* **110,** 695–721, doi:10.1002/qj.49711046509.

Brill, K. F., L. W. Uccellini, R. P. Burkhart, T. T. Warner, and R. A. Anthes, 1985: Numerical simulations of a transverse indirect circulation and low-level jet in the exit region of an upper-level jet. *J. Atmos. Sci.,* **42,** 1306–1320, doi:10.1175/1520-0469(1985)042<1306:NSOATI>2.0.CO;2.

Burpee, R. W., 1972: The origin and structure of easterly waves in the lower troposphere of North Africa. *J. Atmos. Sci.,* **29,** 77–90, doi:10.1175/1520-0469(1972)029<0077:TOASOE>2.0.CO;2.

Cammas, J.-P. W., and D. Ramond, 1989: Analysis and diagnosis of the composition of ageostrophic circulations in jet-front systems. *Mon. Wea. Rev.,* **117,** 2447–2462, doi:10.1175/1520-0493(1989)117<2447:AADOTC>2.0.CO;2.

Cook, K. H., 1999: Generation of the African easterly jet and its role in determining West African precipitation. *J. Climate,* **12,** 1165–1184, doi:10.1175/1520-0442(1999)012<1165:GOTAEJ>2.0.CO;2.

Cornforth, R. J., B. J. Hoskins, and C. D. Thorncoft, 2009: The impact of moist processes on the African easterly jet-African easterly wave system. *Quart. J. Roy. Meteor. Soc.,* **135,** 894–913, doi:10.1002/qj.414.

Danielsen, E. F., 1974: The relationship between severe weather, major dust storms and rapid cyclogenesis. *Synoptic Extratropical Weather Systems,* M. Shapiro, Ed., National Center for Atmospheric Research, 215–241.

Dee, D. P., and Coauthors, 2011: The ERA-Interim reanalysis: Configuration and performance of the data assimilation system. *Quart. J. Roy. Meteor. Soc.,* **137,** 553–597, doi:10.1002/qj.828.

Dhonneur, G., 1981: Cloudy mobile cluster main component of Sahel meteorology (in French). *Meteorologie,* **27,** 75–82.

Diongue, A., J.-P. Lafore, J.-L. Redelsperger, and R. Roca, 2002: Numerical study of a Sahelian synoptic weather system: Initiation and mature stages of convection and its interactions with the large-scale dynamics. *Quart. J. Roy. Meteor. Soc.,* **128,** 1899–1927, doi:10.1256/003590002320603467.

Druyan, L. M., and T. M. Hall, 1996: The sensitivity of African wave disturbances to remote forcing. *J. Appl. Meteor.,* **35,** 1100–1110, doi:10.1175/1520-0450(1996)035<1100:TSOAWD>2.0.CO;2.

Duvel, J.-P., 1989: Convection over tropical Africa and the Atlantic Ocean during northern summer. Part I: Interannual and diurnal variations. *Mon. Wea. Rev.,* **117,** 2782–2799, doi:10.1175/1520-0493(1989)117<2782:COTAAT>2.0.CO;2.

Eldridge, R. H., 1957: A synoptic study of West African disturbance lines. *Quart. J. Roy. Meteor. Soc.,* **83,** 303–314, doi:10.1002/qj.49708335704.

Evaristo, R., G. Scialom, N. Viltard, and Y. Lemaître, 2010: Polarimetric signatures and hydrometeor classification of West African squall lines. *Quart. J. Roy. Meteor. Soc.,* **136,** 272–288, doi:10.1002/qj.561.

Fink, A. H., and A. Reiner, 2003: Spatiotemporal variability of the relation between African easterly waves and West African squall lines in 1998 and 1999. *J. Geophys. Res.,* **108,** 4332, doi:10.1029/2002JD002816.

Fiolleau, T., and R. Roca, 2013: An algorithm for the detection and tracking of tropical mesoscale convective systems using infrared images from geostationary satellite. *IEEE Trans. Geosci. Remote Sens.,* **51,** 4302–4315, doi:10.1109/TGRS.2012.2227762.

Fontaine, B., and S. Janicot, 1992: Wind-field coherence and its variations over West Africa. *J. Climate,* **5,** 512–524, doi:10.1175/1520-0442(1992)005<0512:WFCAIV>2.0.CO;2.

Grist, J. P., and S. E. Nicholson, 2001: A study of the dynamic factors influencing the rainfall variability in the West Africa Sahel. *J. Climate,* **14,** 1337–1359, doi:10.1175/1520-0442(2001)014<1337:ASOTDF>2.0.CO;2.

Hodges, K. I., 1998: Feature-point detection using distance transforms: Application to tracking tropical convective complexes. *Mon. Wea. Rev.,* **126,** 785–795, doi:10.1175/1520-0493(1998)126<0785:FPDUDT>2.0.CO;2.

Hoskins, B. J., M. E. McIntyre, and A. W. Robertson, 1985: On the use and significance of isentropic potential vorticity maps. *Quart. J. Roy. Meteor. Soc.,* **111,** 877–946, doi:10.1002/qj.49711147002.

Houze, R. A., 2004: Mesoscale convective systems. *Rev. Geophys.,* **42,** RG4003, doi:10.1029/2004RG000150.

Huang, H.-C., and K. A. Emanuel, 1991: The effects of evaporation on frontal circulation. *J. Atmos. Sci.,* **48,** 619–628, doi:10.1175/1520-0469(1991)048<0619:TEOEOF>2.0.CO;2.

Krishnamurti, T. N., and H. N. Bhalme, 1976: Oscillations of a monsoon system. Part I: Observational aspects. *J. Atmos. Sci.,* **33,** 1937–1954, doi:10.1175/1520-0469(1976)033<1937:OOAMSP>2.0.CO;2.

Lafore, J.-P., and M. W. Moncrieff, 1989: A numerical investigation of the organization and interaction of the convective and stratiform region of tropical squall lines. *J. Atmos. Sci.,* **46,** 521–544.

Lagouvardos, K., Y. Lemaître, and G. Scialom, 1992: Mesoscale ageostrophic circulations of two fronts observed during the FRONTS87 experiment: Diagnosis and interpretation. *Meteor. Atmos. Phys.,* **48,** 293–307, doi:10.1007/BF01029574.

Laing, A. G., and J. M. Fritsch, 1993: Mesoscale convective complexes in Africa. *Mon. Wea. Rev.,* **121,** 2254–2263, doi:10.1175/1520-0493(1993)121<2254:MCCIA>2.0.CO;2.

——, and ——, 2000: The large-scale environments of the global populations of mesoscale convective complexes. *Mon. Wea. Rev.,* **128,** 2756–2776, doi:10.1175/1520-0493(2000)128<2756:TLSEOT>2.0.CO;2.

——, R. Carbone, V. Levizzani, and J. Tuttle, 2008: The propagation and diurnal cycles of deep convection in northern tropical Africa. *Quart. J. Roy. Meteor. Soc.,* **134,** 93–109, doi:10.1002/qj.194.

——, ——, and ——, 2011: Cycles and propagation of deep convection over equatorial Africa. *Mon. Wea. Rev.,* **139,** 2832–2853, doi:10.1175/2011MWR3500.1.

Lavaysse, C., A. Diedhiou, H. Laurent, and T. Lebel, 2006: African Easterly Waves and convective activity in wet and dry sequences of the West African Monsoon. *Climate Dyn.,* **27,** 319–332, doi:10.1007/s00382-006-0137-5.

Lemaître, Y., 1982: Dynamic and thermodynamic study of tropical squall lines observed in Korhogo during COPT 81 experience (in French). *J. Rech. Atmos.,* **16,** 47–69.

——, and J. Testud, 1986: Observation and modelling of tropical squall lines observed during the ''COPT 79'' Experiment. *Ann. Geophys.,* **4,** 26–36.

——, P. Neveu, and G. Scialom, 1994: A new analysis to diagnose ageostrophic wind from wind and temperature measurements made by an observational network. *J. Atmos. Oceanic Technol.,* **11,** 637–660, doi:10.1175/1520-0426(1994)011<0637:ANATDA>2.0.CO;2.

Leroux, S., and N. M. J. Hall, 2009: On the relationship between African easterly waves and the African easterly jet. *J. Atmos. Sci.,* **66,** 2303–2313, doi:10.1175/2009JAS2988.1.

Ludlam, F. H., 1963: *Severe Local Storms: A Review. Meteor. Monogr.,* No. 27, Amer. Meteor. Soc., 1–30.

Machado, L. A. T., J.-P. Duvel, and M. Desbois, 1993: Diurnal variations and modulation by easterly waves of the size distribution of convective cloud clusters over West Africa and the Atlantic Ocean. *Mon. Wea. Rev.,* **121,** 37–49, doi:10.1175/1520-0493(1993)121<0037:DVAMBE>2.0.CO;2.

Mathon, V., and H. Laurent, 2001: Life cycle of Sahelian mesoscale convective cloud systems. *Quart. J. Roy. Meteor. Soc.,* **127,** 377–406, doi:10.1002/qj.49712757208.

——, ——, and T. Lebel, 2002: Mesoscale convective system rainfall in the Sahel. *J. Appl. Meteor.,* **41,** 1081–1092, doi:10.1175/1520-0450(2002)041<1081:MCSRIT>2.0.CO;2.

Mohr, K. I., and C. D. Thorncroft, 2006: Intense convective systems in West Africa and their relationship to the African easterly jet. *Quart. J. Roy. Meteor. Soc.,* **132,** 163–176, doi:10.1256/qj.05.55.

——, J. S. Famiglietti, and E. J. Zipser, 1999: The contribution to tropical rainfall with respect to convective system type, size, and intensity estimated from the 85-GHz ice-scattering signature. *J. Appl. Meteor.,* **38,** 596–606, doi:10.1175/1520-0450(1999)038<0596:TCTTRW>2.0.CO;2.

Moncrieff, M. W., and E. Klinker, 1997: Organized convective systems in the tropical western Pacific as a process in general circulation models: A TOGA COARE case-study. *Quart. J. Roy. Meteor. Soc.,* **123,** 805–827, doi:10.1002/qj.49712354002.

Moore, J. T., and G. E. VanKnowe, 1992: The effect of jet-streak curvature on kinematic fields. *Mon. Wea. Rev.,* **120,** 2429–2441, doi:10.1175/1520-0493(1992)120<2429:TEOJSC>2.0.CO;2.

Mounier, F., G. N. Kiladis, and S. Janicot, 2007: Analysis of the dominant mode of convectively coupled Kelvin waves in the West African monsoon. *J. Climate,* **20,** 1487–1503, doi:10.1175/JCLI4059.1.

——, S. Janicot, and G. N. Kiladis, 2008: The West African Monsoon dynamics. Part III: The quasi-biweekly zonal dipole. *J. Climate,* **21,** 1911–1928, doi:10.1175/2007JCLI1706.1.

Namias, J., and P. F. Clapp, 1949: Confluence theory of the high tropospheric jet stream. *J. Meteor.,* **6,** 330–336, doi:10.1175/1520-0469(1949)006<0330:CTOTHT>2.0.CO;2.

Newell, R. E., and J. W. Kidson, 1984: African mean wind changes between Sahelian wet and dry periods. *J. Climatol.,* **4,** 27–33, doi:10.1002/joc.3370040103.

Newton, C. W., 1963: *Dynamics of Severe Convective Storms. Meteor. Monogr.,* No. 27, Amer. Meteor. Soc., 33–55.

——, 1967: Severe convection storms. *Advances in Geophysics,* Vol. 12, Academic Press, 257–303, doi:10.1016/S0065-2687(08)60377-5.

Nicholls, S. D., and K. I. Mohr, 2010: An analysis of the environments of intense convective systems in West Africa in 2003. *Mon. Wea. Rev.,* **138,** 3721–3739, doi:10.1175/2010MWR3321.1.

Nicholson, S. E., 2009: On the factors modulating the intensity of the tropical rainbelt over West Africa. *Int. J. Climatol.,* **29,** 673–689, doi:10.1002/joc.1702.

——, and J. P. Grist, 2003: The seasonal evolution of the atmospheric circulation over West Africa and equatorial Africa. *J. Climate,* **16,** 1013–1030, doi:10.1175/1520-0442(2003)016<1013:TSEOTA>2.0.CO;2.

Nieto-Ferreira, R., T. Rickenbach, N. Guy, and E. Williams, 2009: Radar observation of convective system variability in relationship to African easterly waves during the 2006 AMMA special observing period. *Mon. Wea. Rev.,* **137,** 4136–4150, doi:10.1175/2009MWR2740.1.

Palmèn, E., and C. W. Newton, 1969: *Atmospheric Circulation Systems: Their Structure and Physical Interpretation.* Academic Press, 602 pp.

Parker, D. J., C. D. Thorncroft, R. R. Burton, and A. Diongue-Niang, 2005: Analysis of the African easterly Jet, using aircraft observations from the JET2000 Experiment. *Quart. J. Roy. Meteor. Soc.,* **131,** 1461–1482, doi:10.1256/qj.03.189.

Payne, S. W., and M. M. McGarry, 1977: The relationship of satellite inferred convective activity to easterly waves over West Africa and the adjacent ocean during Phase III of GATE. *Mon. Wea. Rev.,* **105,** 413–420, doi:10.1175/1520-0493(1977)105<0413:TROSIC>2.0.CO;2.

Petterssen, S., 1956: *Motion and Motion Systems.* Vol. 2, *Weather Analysis and Forecasting,* McGraw-Hill, 428 pp.

Protat, A., and Y. Lemaître, 2001: Scale interactions involved in the initiation, structure, and evolution of the 15 December 1992 MCS observed during TOGA-COARE. Part I: Synoptic-scale processes. *Mon. Wea. Rev.,* **129,** 1757–1778, doi:10.1175/1520-0493(2001)129<1757:SIIITI>2.0.CO;2.

Redelsperger, J.-L., A. Diongue, A. Diedhou, J.-P. Céron, M. Diop, J.-F. Guérémy, and J.-P. Lafore, 2002: Multi-scale description of a Sahelian synoptic weather system representative of the West African Monsoon. *Quart. J. Roy. Meteor. Soc.,* **128,** 1229–1257, doi:10.1256/003590002320373274.

Reiter, E. R., 1963: *Jet-Stream Meteorology.* The University of Chicago Press, 515 pp.

——, 1969: Tropospheric circulation and jet streams. *Climate of the Free Atmosphere,* D. F. Rex, Ed., Vol. 4, *World Survey of Climatology,* Elsevier, 85–203.

Rickenbach, T., R. Nieto-Ferreira, N. Guy, and E. Williams, 2009: Radar-observed squall line propagation and the diurnal cycle of convection in Niamey, Niger, during the 2006 African Monsoon and Multidisciplinary Analyses intensive observing period. *J. Geophys. Res.,* **114,** D03107, doi:10.1029/2008JD010871.

Rotunno, R., J. B. Klemp, and M. L. Weisman, 1988: A theory for strong, long-lived squall lines. *J. Atmos. Sci.,* **45,** 463–485, doi:10.1175/1520-0469(1988)045<0463:ATFSLL>2.0.CO;2.

Rowell, D. P., and J. R. Milford, 1993: On the generation of African squall lines. *J. Climate,* **6,** 1181–1193, doi:10.1175/1520-0442(1993)006<1181:OTGOAS>2.0.CO;2.

Scialom, G., and Y. Lemaître, 2011: Vertical moistening by AMMA mesoscale convective systems. *J. Atmos. Oceanic Technol.,* **28,** 617–639, doi:10.1175/2010JTECHA1486.1.

——, J. Faroux, M. Giraud, R. Ney, R. Evaristo, Y. Lemaître, and N. Viltard, 2009: RONSARD radar: Implementation of dual polarization on a C-band Doppler weather radar. *IEEE Geosci. Remote Sensing Lett.,* **6,** 132–136, doi:10.1109/LGRS.2008.2008318.

Tetzlaff, G., and M. Peters, 1988: A composite study of early summer squall lines and their environment over West Africa. *Meteor. Atmos. Phys.,* **38,** 153–163, doi:10.1007/BF01029779.

Thorncroft, C. D., and M. Blackburn, 1999: Maintenance of the African easterly jet. *Quart. J. Roy. Meteor. Soc.,* **125,** 763–786, doi:10.1002/qj.49712555502.

——, J.-P. Lafore, G. Berry, R. Roca, M. T. F. Guichard, and N. Asencio, 2007: Overview of African weather systems during the summer 2006. *CLIVAR Exchanges,* No. 41, International CLIVAR Project Office, Southampton, United Kingdom, 18–20.

Thorpe, A. J., and K. A. Emanuel, 1985: Frontogenesis in the presence of small stability to slantwise convection. *J. Atmos. Sci.,* **42,** 1809–1824, doi:10.1175/1520-0469(1985)042<1809:FITPOS>2.0.CO;2.

Uccellini, L. W., and D. R. Johnson, 1979: The coupling of upper and lower tropospheric jet streaks and implication for the development of severe convective storms. *Mon. Wea. Rev.,* **107,** 682–703, doi:10.1175/1520-0493(1979)107<0682:TCOUAL>2.0.CO;2.

——, and P. J. Kocin, 1987: The interaction of jet streak circulations during heavy snow events along the East Coast of the United States. *Wea. Forecasting,* **2,** 289–308, doi:10.1175/1520-0434(1987)002<0289:TIOJSC>2.0.CO;2.

Van de Berg, L., T. Heinemann, M. Szyndel, L. von Bremen, M. König, C. Rogers, P. Pili, and A. Yildrim, 2003: The calibration of the infrared channels of METEOSAT First and Second Generation spacecraft. *Proc. EUMETSAT Meteorological Satellite Conf.,* Weimar, Germany, EUMETSAT, EUM-P-39.

Xu, Q., 1989: Frontal circulations in the presence of small viscous moist symmetric stability and weak forcing. *Quart. J. Roy. Meteor. Soc.,* **115,** 1325–1353, doi:10.1002/qj.49711549008.